

Article

Three-Color White Photoluminescence Emission Using Perovskite Nanoplatelets and Organic Emitter

Hyukmin Kwon [†], Sunwoo Park [†], Seokwoo Kang, Hayoon Lee and Jongwook Park ^{*}

Integrated Engineering, Department of Chemical Engineering, Kyung Hee University, Yongin 17104, Korea; hm531@khu.ac.kr (H.K.); mdrafix@khu.ac.kr (S.P.); swkang@khu.ac.kr (S.K.); kssarang1@khu.ac.kr (H.L.)

^{*} Correspondence: jongpark@khu.ac.kr

[†] These authors contributed equally to this work.

Abstract: Three organic blue-light-emitting tetraphenylethylene (TPE) derivatives that exhibit aggregation-induced emission (AIE) were used as additives in the preparation of inorganic perovskite-structured green-light-emitting materials for three-color white-light emission. For these organic-inorganic light-emitting materials, two-color (blue and green) light-emitting films based on the CsPbBr₃ perovskite-structured green-light-emitting inorganic material were prepared. The three TPE derivatives were prepared by varying the number of bromide groups, and a distinct AIE effect was confirmed when the derivatives were dissolved in a water–tetrahydrofuran mixed solvent containing 90 vol% water. When 0.2 molar ratio of the 1,1,2,2-tetrakis(4-bromophenyl)ethylene (TeBrTPE) additive was mixed with nanocrystal-pinning toluene solvent, the green-light-emission photoluminescence quantum efficiency (PLQY) value at 535 nm was 47 times greater than that of the pure bulk CsPbBr₃ without additives and a blue emission at 475 nm was observed from the TeBrTPE itself. When a CBP:Ir(piq)₃ film was prepared on top of this layer, three PL peaks with maximum wavelength values of 470, 535, and 613 nm were confirmed. The film exhibited white-light emission with CIE color coordinates of (0.25, 0.36).

Keywords: aggregation-induced emission; metal halide perovskite; tetraphenylethylene; three-color white emission



Citation: Kwon, H.; Park, S.; Kang, S.; Lee, H.; Park, J. Three-Color White Photoluminescence Emission Using Perovskite Nanoplatelets and Organic Emitter. *Molecules* **2022**, *27*, 3982. <https://doi.org/10.3390/molecules27133982>

Academic Editors: Youhong Tang and Elias Stathatos

Received: 7 June 2022

Accepted: 20 June 2022

Published: 21 June 2022

Publisher's Note: MDPI stays neutral with regard to jurisdictional claims in published maps and institutional affiliations.



Copyright: © 2022 by the authors. Licensee MDPI, Basel, Switzerland. This article is an open access article distributed under the terms and conditions of the Creative Commons Attribution (CC BY) license (<https://creativecommons.org/licenses/by/4.0/>).

1. Introduction

Organic light-emitting diode (OLED) technology has grown into a representative display technology over the past 30 years because of its advantages of high electroluminescence (EL) efficiency, high resolution, and low energy consumption and because it can be applied to this and light flexible displays [1–4]. However, the high material cost and low color purity of organic emitters used in OLEDs are major obstacles to product development and to the realization of devices that display vivid and natural colors. To address these problems, researchers have widely investigated AMX₃-based metal halide perovskites (MHPs) for use in light-emitting diodes (LEDs), photodetectors, and photovoltaic applications because of their narrow full-width at half-maximum (FWHM) emission band, excellent color purity and charge carrier mobility, tunable optical bandgap, and easy preparation via solution processes [5–11]. Here, *A* is an organic or inorganic cation such as methylammonium (MA⁺), formamidinium (FA⁺), or Cs⁺; *M* is a divalent metal cation such as Pb²⁺ or Sn²⁺; and *X* is a halide such as Cl[−], Br[−], or I[−]. However, defect sites on the surface of MHPs adversely affect both their optical and electrical properties. Consequently, researchers have passivated the defect sites of nanocrystals with specific materials such as organic ligands, inorganic species, or polymers to enhance the photoluminescence (PL) intensity of MHP materials and improve the operating stability of perovskite-based LEDs [12,13]. Representative organic ligands are MA, FA, and phenylethylammonium (PEA⁺) which are small organic-salt-type ligands [14–16]. In addition, small metal cations used for passivation, such as Na⁺ ions, have a smaller ionic radius than the metal ions in

the perovskite component, enabling the small metal cations to occupy interstitial sites or lattice vacancies and easily passivate the defect sites [17].

Unlike previously reported studies in which perovskite materials were prepared with ammonium derivatives, the present work aims to improve the luminescence properties of perovskite materials by incorporating light-emitting organic compounds that exhibit aggregation-induced emission (AIE). Organic emitter derivatives based on anthracene, pyrene, or perylene chromophores, which are generally used for OLEDs, exhibit high emission efficiency in dilute solutions but weak emission in the aggregated film state because of the aggregation-caused quenching effect [18–20]. However, some new luminescent materials have an opposite effect, demonstrating bright-light emission upon aggregation in the film state. Typically, tetraphenylethylene (TPE) derivatives have a propeller-shaped structure that is a representative chemical structure exhibiting AIE characteristics [21–27]. Therefore, in the present study, we focus on new additives for perovskite-based light-emitting material components by using TPE and Br-substituted TPE derivatives to improve the PL light-emitting performance of film-state perovskites.

White LEDs (WLEDs) are important for lighting and display applications; however, perovskite-based WLEDs have rarely been reported. Recently, perovskite-based WLEDs with organic light-emitting materials have been reported to emit white light with two or three wavelengths through a single emitting layer or a double emitting layer [28–33]. One potential approach to achieving white-light electroluminescence through a single emitting layer is to use a perovskite emitter mixed with organic molecules such as small molecules or polymers. However, this method can realize only two-color white-light emission based on blue and yellow, not three-color white-light emission based on red, green, and blue. Three separate primary colors are basically required for a full-color display.

Because TPE derivatives emit in the blue region and CsPbBr₃ emits in the green region, two-color emission of this mixed state can be applied as a component of three-color emission. In addition, if a red-emitting layer is placed on top of a two-color emissive layer, three-color white emission can be attained. We used this approach in the present study. Specifically, we used a solution process to fabricate an organic–inorganic mixed film capable of simultaneously emitting blue and green light and subsequently realized three-color white PL emission of a double layer by depositing tris(1-phenylisoquinoline)iridium(III) (Ir(piq)₃), a red-light-emitting material, onto the two-color emissive layer. The results suggest that three-color white EL emission is feasible.

2. Experimental Section

2.1. Synthesis

2.1.1. 1-Bromo-4-(1,2,2-triphenylethylene)benzene

Diphenylmethane (2.02 g, 12.00 mmol) was dissolved in 30 mL dry tetrahydrofuran (THF) and cooled to $-5\text{ }^{\circ}\text{C}$ in an ice bath. *n*-Butyllithium solution (6.25 mL, 5.50 mmol, 1.6 M in *n*-hexane) was added dropwise to the diphenylmethane solution, and the resultant mixture was stirred at $-5\text{ }^{\circ}\text{C}$ for 30 min. 4-Bromobenzophenone (2.35 g, 9.00 mmol) was added under a N₂ atmosphere, the ice bath was removed, and the reaction mixture was warmed to room temperature and stirred at this temperature for 6 h. Afterwards, 50 mL of a saturated ammonium chloride solution was added and extracted with a dichloromethane–distilled water solution. The organic layer was dried over anhydrous MgSO₄, and the solution was concentrated under reduced pressure. The crude product was used without further purification during the following reaction step and was placed under a N₂ atmosphere and dissolved in 80 mL of toluene; *para*-toluene sulfonic acid (0.342 g, 1.8 mmol) was then added. The reaction mixture was heated to 120 °C and stirred at this temperature for 12 h. When the reaction was completed, the crude product was extracted with CH₂Cl₂–distilled water. The organic layer was dried over anhydrous MgSO₄, and the solution was concentrated under reduced pressure. After column purification using ethyl acetate:hexane = 1:100, reprecipitation from THF and methanol gave a white solid. (47% yield) ¹H NMR (400 MHz, DMSO): δ (ppm) 7.30–7.28 (m, 2H), 7.15–7.05 (m, 9 H),

6.95–6.91 (m, 6 H), 6.87–6.85 (m, 2 H). ^{13}C NMR (101 MHz, DMSO): δ 143.42, 143.37, 143.21, 143.01, 141.77, 139.84, 133.31, 131.35, 131.18, 131.16, 131.09, 128.55, 128.49, 128.39, 127.36, 127.29, 127.24, 120.30 ppm. HRMS (FAB-MS, m/z): calcd. for $\text{C}_{26}\text{H}_{19}\text{Br}$, 410.07; found, 410.412 $[\text{M}]^+$.

2.1.2. 1,1,2,2-Tetrakis(4-bromophenyl)ethylene (TeBrTPE)

Bromine (9.6 g, 60.00 mmol) was added to a solution of tetraphenylethylene (2.50 g, 7.50 mmol) in 15 mL of glacial acetic acid and 30 mL of methylene chloride at 0 °C. The resultant mixture was stirred at room temperature for 4 h, poured into 100 mL ice water and extracted with CH_2Cl_2 . The organic product was washed with water, brine and then dried over MgSO_4 ; the solvent was subsequently removed under reduced pressure. The crude product was purified by recrystallization from methanol to give 1,1,2,2-tetrakis(4-bromophenyl)ethylene (TeBrTPE) as a white solid. (92% yield) ^1H NMR (400 MHz, DMSO): δ (ppm) 7.37–7.34 (m, 8H), 6.90–6.86 (m, 8 H). ^{13}C NMR (101 MHz, DMSO): δ 141.99, 139.85, 133.29, 131.68, 120.98 ppm. HRMS (FAB-MS, m/z): calcd. for $\text{C}_{26}\text{H}_{16}\text{Br}_4$, 643.80; found, 644.185 $[\text{M}]^+$.

2.2. Materials and Instruments

Diphenylmethane, *n*-Butyllithium solution (1.6 M in *n*-hexane), 4-Bromobenzophenone, TPE, 9,10-dibromoanthracene (9,10-DBA), cesium bromide (CsBr), lead(II) bromide (PbBr_2), anhydrous dimethyl sulfoxide (DMSO), and toluene were purchased from Sigma-Aldrich. Hydrobromic acid (HBr) solution (48% in water) was purchased from Alfa Aesar. All chemicals were used without further purification. Optical absorption spectra were recorded using a Hewlett-Packard 8453 ultraviolet–visible–near-infrared (UV–Vis–NIR) spectrophotometer. The ^1H NMR spectra were recorded on Bruker Advance 400 spectrometers (Bruker, Billerica, MA, USA). The FAB \pm mass was recorded on a JMS-700. A Perkin-Elmer LS55 luminescence spectrometer (Perkin-Elmer, Waltham, MA, USA, light source: 20 kw pulsed Xe flash tube, filter: 1%, slit width: 10:10 nm) was used to record PL spectra. Absolute photoluminescence quantum yield (PLQY) values were obtained using a Quantaury-QY quantum yield spectrometer (Hamamatsu photonics, Hamamatsu, Japan). The time-resolved fluorescence data were obtained using a Hamamatsu Photonics C11367-11 fluorescence lifetime spectrometer (Hamamatsu photonics, Hamamatsu, Japan). The average lifetimes of the emission decay were obtained by the equation [34]. X-ray diffraction (XRD) data were obtained using a Bruker D8 Advance diffractometer (Bruker, Billerica, MA, USA). Scanning electron microscopy (SEM) images were obtained using a JEM-2100F (JEOL, Toyko, Japan) electron microscope operating at 200 kV. CIE color coordinates of the perovskite organic film were measured at room temperature and under ambient conditions using a Konica Minolta CS-100 spectroradiometer (Konica Minolta, Toyko, Japan).

2.3. Perovskite Solution Preparation

CsPbBr_3 powder was prepared and used as one of the starting materials for film preparation. We dissolved PbBr_2 (10 mmol, 3.67 g) in HBr (8 mL), to which we then slowly added CsBr (10 mmol, 2.12 g, dissolved in 3 mL of water), resulting in an orange precipitate. The precipitate was filtered, washed twice with ethanol, and dried at 60 °C in a vacuum oven for 12 h before use. The synthesized CsPbBr_3 (0.3 mmol, 0.174 g) was dissolved in 1 mL of DMSO to prepare a perovskite solution. Nanocrystal-pinning (NCP) toluene solvent was then mixed with different amounts of TPE or its derivatives (i.e., BrTPE and TeBrTPE). For example, to prepare a non-solvent having a 1:1 CsPbBr_3 -to-TPE mole concentration ratio, a mass of 0.099 g (0.3 mmol) of TPE was dissolved in toluene.

2.4. Perovskite Films Preparation

Glass substrates (25 mm \times 25 mm) were sequentially washed by ultrasonication in acetone, ethanol, deionized water, and isopropyl alcohol and then dried in an oven at 80 °C. The substrates were further cleaned with a UV–ozone cleaner for 10 min before the

spin-coating process. A CsPbBr₃ solution was spin-coated at 3000 rpm for a total of 60 s; at the midpoint of the spin-coating process (i.e., after 30 s), 0.2 mL of NCP toluene solvent including TPE or one of its derivatives was dropped onto the surface; the coated substrate was then heat-treated at 70 °C for 1 min.

3. Results and Discussion

3.1. AIE Characterization of TPE Derivatives

Among the numerous organic materials that can potentially be added to perovskite light-emitting materials, we used organic materials that exhibited AIE properties to achieve the three-wavelength PL phenomenon. As shown in Figure 1, three TPE derivatives were selected and synthesized in the present study because TPE-based compounds are easy to synthesize and because the halide substitution effect enables the change in luminescence properties depending on the AIE properties to be easily characterized. The synthesized compounds were characterized using NMR spectroscopy (Figures S1–S4). Because TPE has a large bandgap such as 3.7 eV, it emits in the blue region (467 nm) in the solution state [35]. BrTPE and TeBrTPE show PL maxima of 482 and 490 nm, which are bathochromically shifted compared with that of TPE; however, these results show that the large bandgap and blue emission of TPE are retained even when one or more halide atoms are substituted into its structure.

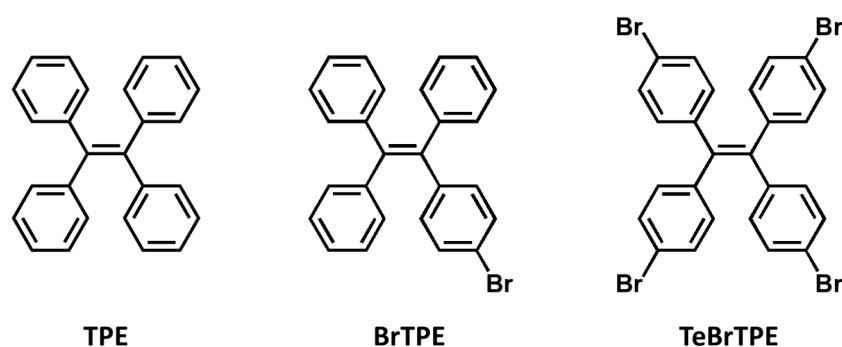


Figure 1. The chemical structures of the synthesized TPE derivatives used as organic spacers in CsPbBr₃ films.

To investigate the AIE characteristics of TPE, BrTPE, and TeBrTPE, we recorded the PL spectra of samples prepared using a mixture of THF as a good solvent and H₂O as a non-solvent. Figure 2 and Figure S5 shows the PL spectra of the TPE derivatives in a THF–water solvent with a water fraction (f_w) of 90 vol%. In water fraction (f_w) of 90 vol%, PL maximum peak of TPE is 465 nm. In the case of BrTPE, the emission peak of BrTPE was observed at 485 nm, which was redshifted by ~20 nm from that of TPE. In the case of TeBrTPE, the emission peak appeared at 490 nm, which was redshifted by ~25 nm from that of TPE. When we use PLQY measurement in solution state, it is very difficult to measure the clear value due to the low PL quantum yield.

3.2. Optical Properties of Organic–Inorganic CsPbBr₃ Nanoplatelet Films with an Organic Emitter

Figure 3 shows the ultraviolet–visible absorption spectra of the CsPbBr₃ films containing TPE derivatives at various molar ratios. The spectrum of the bulk CsPbBr₃ shows broad absorption at wavelengths less than 530 nm, and the films with TPE-derivative/CsPbBr₃ molar ratios of 0.2–0.6 show a TPE absorption peak at ~315 nm. Bulk perovskite has been reported to exhibit absorption in the 430–470 nm range when transformed into a 2D low-dimensional phase by the addition of organic ligands [11,36]. However, when TPE and the Br-substituted TPE derivatives were added to CsPbBr₃, a new absorption peak at 430–470 nm was not observed. The non-normalized PL spectra and the related optical properties of the CsPbBr₃ films with different molar ratios of CsPbBr₃ and TPE derivatives are shown in Figure 4, Figure S7, and Table 1, respectively. The spectrum of the pure

CsPbBr₃ film shows a weak maximum PL peak at 535 nm. When the TPE/CsPbBr₃ molar ratio was increased from 0.2 to 0.6, two emission peaks were confirmed: one at 446 nm, which was the emission peak of TPE, and one at 535 nm, which was the emission peak of CsPbBr₃. In the case of BrTPE, the emission peak of BrTPE was observed at 471 nm, which was redshifted by ~5 nm from that of TPE. In the case of TeBrTPE, the emission peak appeared at 476 nm, which was redshifted by ~9 nm from that of TPE. These results are attributed to enhancements in both the interaction of the TPE compound and CsPbBr₃ and the grain-boundary defect passivation of CsPbBr₃ with increasing number of bromides and increasing amount of the TeBrTPE derivative. Figure 4d shows a plot of the absolute PLQY ratio (I/I_0) as a function of the molar ratio of TPE derivatives.

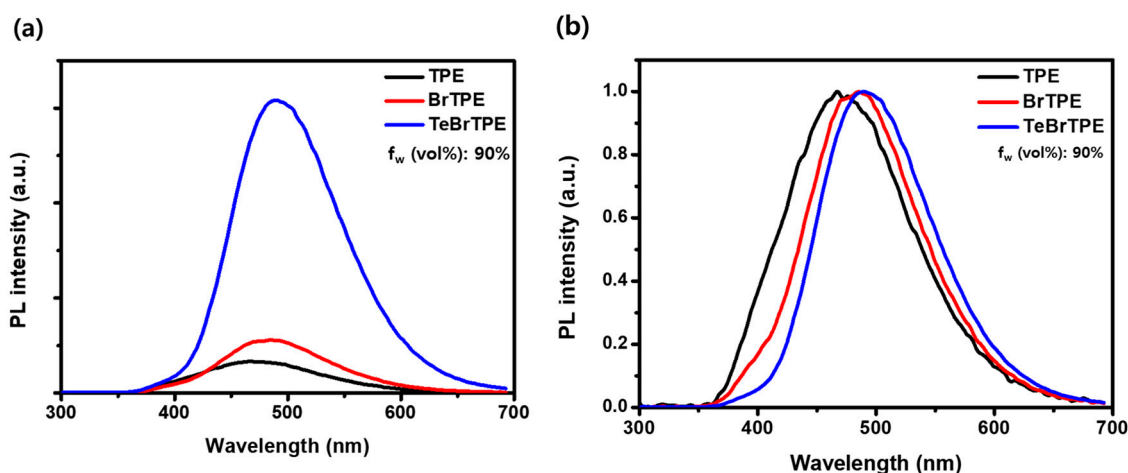


Figure 2. (a) Fluorescence spectra of TPE derivatives in THF (10 vol%) and water (90 vol%) solvents; (b) Normalized fluorescence spectra of TPE derivatives in THF (10 vol%) and water (90 vol%) solvents.

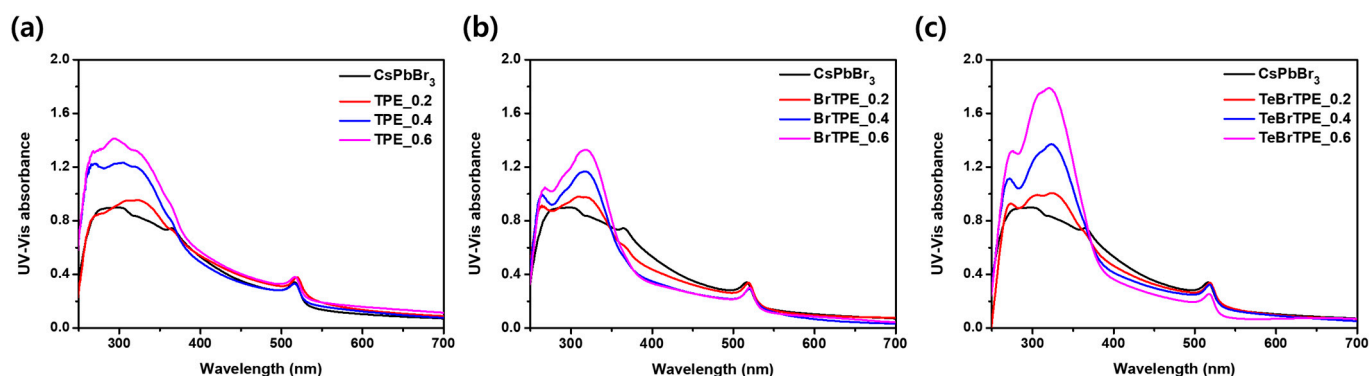


Figure 3. Absorption spectra of perovskite films with various molar ratios of TPE derivatives: (a) CsPbBr₃ perovskite films with TPE/CsPbBr₃ molar ratios of 0.2, 0.4, and 0.6; (b) CsPbBr₃ perovskite films with BrTPE/CsPbBr₃ molar ratios of 0.2, 0.4, and 0.6; and (c) CsPbBr₃ perovskite films with TeBrTPE/CsPbBr₃ molar ratios of 0.2, 0.4, and 0.6.

Table 1 shows the PL properties of the CsPbBr₃ films containing the TPE compounds. The absolute PLQY of all the samples was measured at 535 nm (i.e., the green emission region); the pure CsPbBr₃ film showed a PLQY of 0.4%. When TPE was added at molar ratios of 0.2, 0.4, and 0.6, the PLQY values increased to 0.7%, 1.2%, and 1.2%, respectively; however, no substantial difference was observed in the PLQY values of the TPE additive cases. However, when the BrTPE additive was added at the same concentrations as the TPE additive, the PLQY was 5.9%, 9.6%, and 13.8%; in addition, we confirmed that the PLQY was improved approximately tenfold compared with that when TPE was added. Furthermore, when TeBrTPE was added to the CsPbBr₃ film at the same molar ratios, high PLQY values of 12.2%, 16.2%, and 18.6% were attained, consistent with the PL intensities in Figure 4.

These values are approximately 47 times greater than the PLQY values corresponding to pure CsPbBr₃. The related data showed an error range of less than 5%. Thus, we confirmed that the luminous efficiency of CsPbBr₃ was improved because of AIE, and that two-color (blue and green) emission was realized through optimization of the ratio between the TPE derivatives and the perovskite material.

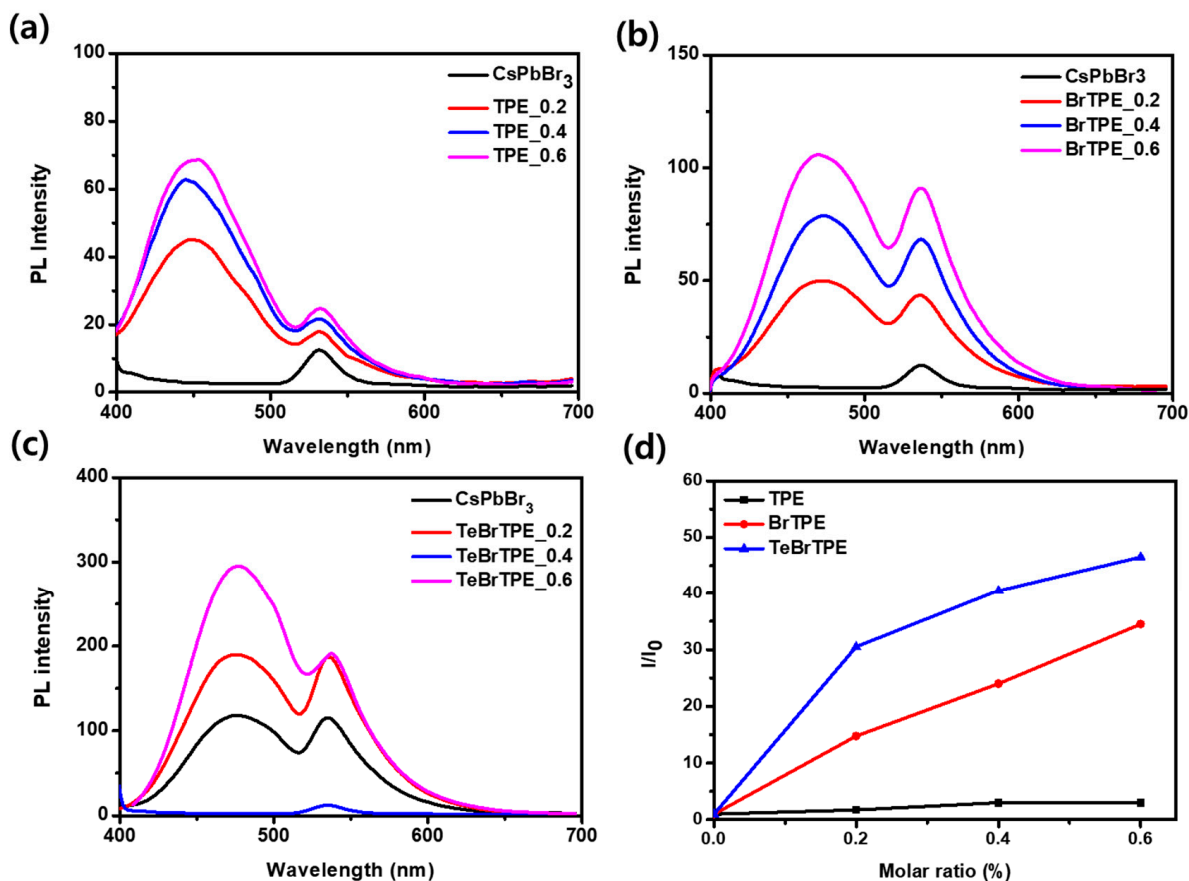


Figure 4. Photoluminescence (PL) spectra of CsPbBr₃ films containing various TPE derivatives: (a) CsPbBr₃ perovskite films with TPE/CsPbBr₃ molar ratios of 0.2, 0.4, and 0.6; (b) CsPbBr₃ perovskite films with BrTPE/CsPbBr₃ molar ratios of 0.2, 0.4, and 0.6; and (c) CsPbBr₃ perovskite films with TeBrTPE/CsPbBr₃ molar ratios of 0.2, 0.4, and 0.6. (d) Plot of the relative emission intensity (I/I_0) as a function of the molar ratio of TPE derivatives, where I is the absolute PLQY value at 535 nm and I_0 is the absolute PLQY value at 535 nm in the spectrum of a pure CsPbBr₃ film (excitation wavelength: 365 nm).

Table 1. Summary of the PL Peak Wavelength, PLQY, and τ_{avg} of CsPbBr₃ Including Various Relative Molar Amounts of TPE Compounds in the Film State.

CsPbBr ₃	TPE Compound and Its Molar Ratio	PL Peak(s) (nm)	PLQY (%) (at 535 nm)	τ_{avg} (ns) (at 535 nm)
1.0	—	535	0.4	0.85
1.0	TPE 0.2	446, 535	0.7	1.78
1.0	TPE 0.4	446, 536	1.2	1.86
1.0	TPE 0.6	446, 536	1.2	2.08
1.0	BrTPE 0.2	471, 535	5.9	5.16
1.0	BrTPE 0.4	472, 535	9.6	5.29
1.0	BrTPE 0.6	472, 536	13.8	5.55
1.0	TeBrTPE 0.2	475, 534	12.2	4.04
1.0	TeBrTPE 0.4	475, 535	16.2	4.25
1.0	TeBrTPE 0.6	464, 535	18.6	4.57

3.3. Morphologies of Organic–Inorganic CsPbBr₃ Nanoplatelet Films with an Organic Emitter

In general, low-dimensional perovskite materials of two-dimensional (2D) and colloidal nanocrystal types with a large exciton binding energy and good film morphology are used to improve the emission efficiency of perovskite materials. In bulk-type perovskite materials, the emission intensity is weak; however, with the addition of an organic ammonium salt to induce a nanoplatelet shape through dimensional engineering and reduce the grain size, the exciton-binding energy can be increased, and the emission efficiency can be improved [37–39]. In the case of perovskite nanocrystals, the emission intensity can be improved by converting a bulk perovskite material into its corresponding perovskite quantum-dot form using long-chain organic ligands such as oleic acid and oleylamine [40,41]. The TPE derivatives used in the present study have not been previously used as a passivation additive. The TPE derivatives even exhibit light-emitting properties as well as AIE properties. XRD and SEM analyses were conducted to investigate the effects of the TPE derivatives on the dimensions of the formed perovskite and the morphology of the corresponding perovskite films.

The XRD patterns of CsPbBr₃ films containing TPE, BrTPE, and TeBrTPE at molar ratios from 0.2 to 0.6 are shown in Figure 5a–c, respectively. The pattern of the pure CsPbBr₃ thin film shows peaks at 2θ values of 15.3°, 21.7°, and 30.1°, which correspond to the (100), (110), and (200) planes of the three-dimensional perovskite structure. Interestingly, as the molar ratio of the TPE derivatives was increased, the intensity of the (110) diffraction peak decreased and the intensities of the (100) and (200) diffraction peaks increased. In the patterns of the films containing TPE, the (100) and (200) diffraction peaks slightly increased compared with those of bulk CsPbBr₃. However, when BrTPE and TeBrTPE were added, the diffraction peak intensities of the (100) and (200) planes clearly increased with increasing molar ratio of the TPE derivatives. In particular, the strongest diffraction peak intensities were observed for TeBrTPE with a TeBrTPE/CsPbBr₃ molar ratio of 0.6. This result means that the bromide of the TPE derivatives contained in the CsPbBr₃ film can be predominantly passivated on the (100) and (200) crystal planes of CsPbBr₃ crystallites and promote the growth of CsPbBr₃ nanoplatelets along the (100) direction as well as the stacked formation [42]. Therefore, with increasing content of the TPE derivatives, the crystallinity of CsPbBr₃ tended to increase along with the PL intensity. In general, the XRD peak corresponding to dimensional control of CsPbBr₃ appears at a 2θ angle of 5°. When the TPE derivative was added, the dimension-controlled XRD peak at 5° was not observed irrespective of the derivative's molar ratio. The same result has been reported by Li and coworkers [42,43].

SEM was used to analyze the changes in the CsPbBr₃ film morphology depending on the addition of TPE derivatives (Figure 5d). The pure CsPbBr₃ film contains pinholes and large crystal domains. When TPE was added to CsPbBr₃ at molar ratios of 0.2, 0.4, and 0.6, the pinholes and grain size decreased but the surface uniformity worsened. When BrTPE or TeBrTPE was added to CsPbBr₃ at molar ratios of 0.2, 0.4, and 0.6, the number of pinholes decreased, and defect passivation was observed. This difference in SEM observations of CsPbBr₃ containing BrTPE and TeBrTPE compared with those of the CsPbBr₃ containing TPE is attributable to the aggregation effect of TPE derivatives as well as to the interaction between TPE derivatives and CsPbBr₃.

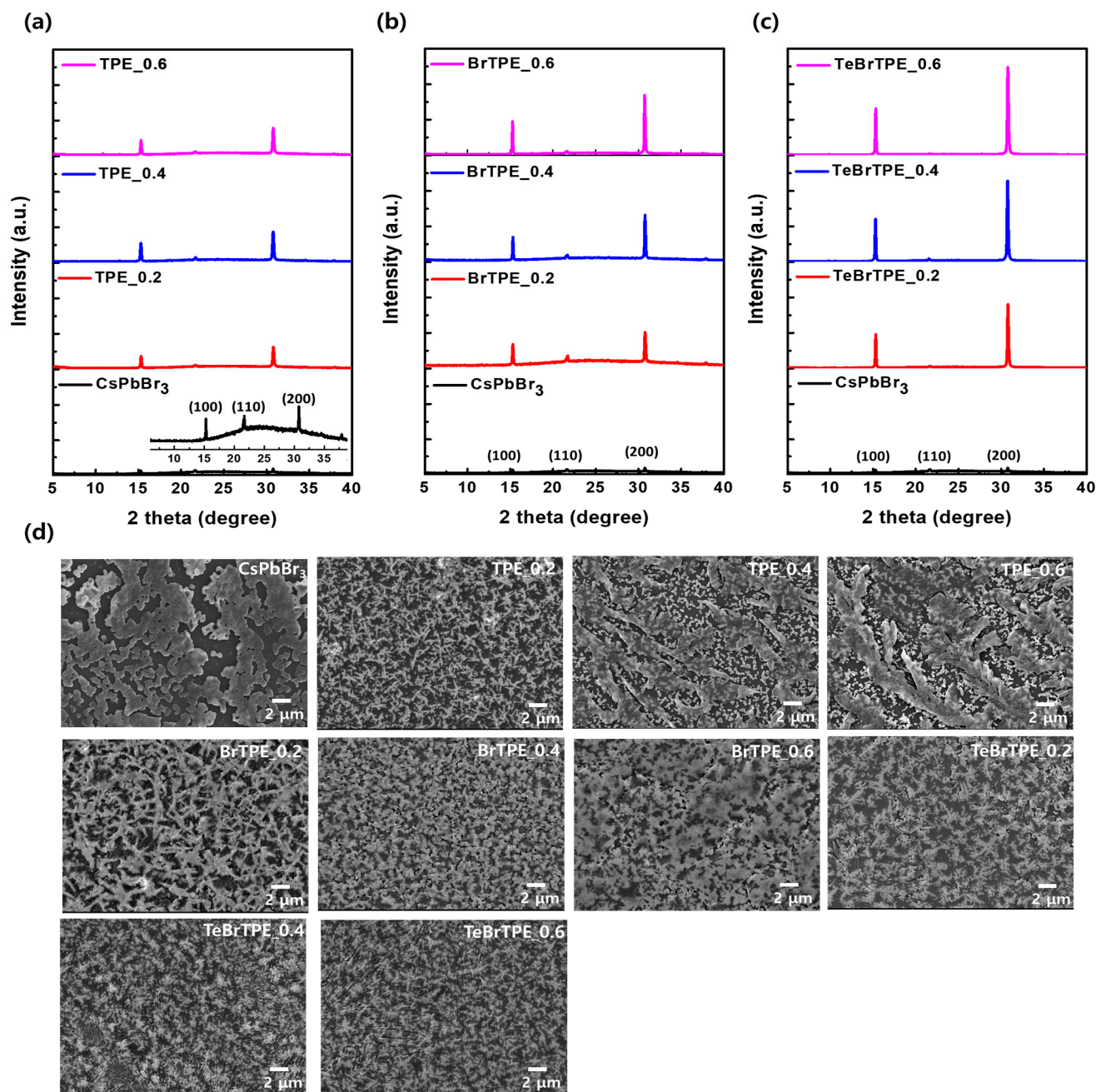


Figure 5. Crystal structures and morphologies of CsPbBr₃ thin films with 0.2, 0.4, and 0.6 mol of TPE, BrTPE, and TeBrTPE per mole of CsPbBr₃. (a–c) X-ray diffraction (XRD) patterns and (d) top-view scanning electron microscopy (SEM) images (25,000 \times , scale bar: 2 μ m).

As a result, the luminous efficiency of CsPbBr₃ samples containing a TPE derivative could increase, which can be explained by three factors. The first factor is the AIE effect of the TPE compounds. The PLQY of CsPbBr₃ films containing TPE derivatives was improved compared with that of a pure CsPbBr₃ film (Table 1). 9,10-DBA, an anthracene derivative without AIE properties, was added to a CsPbBr₃ film under the same conditions to investigate whether the AIE property of the TPE improved the luminous efficiency of the CsPbBr₃ film. The PL properties of these films were investigated; the PL spectra are shown in Figure S8. Anthracene is a chromophore widely used in OLEDs because it has a high PLQY as a blue-light-emitting material. However, the results for films with various molar ratios of 9,10-DBA show that the PL intensity of CsPbBr₃ did not increase; a PL intensity similar to that of bulk CsPbBr₃ was observed. These results indicate that the AIE effect

of the TPE derivatives enhanced the PL intensity of the CsPbBr₃ films. The second factor is the improvement in the luminous efficiency of CsPbBr₃ by the interaction of CsPbBr₃ with the Br substituted onto TPE. We previously confirmed that the PL intensity and PLQY increased in the order TPE, BrTPE, and TeBrTPE. In addition, the decay time of the light intensity based on the PL mission at 535 nm confirmed that an interaction occurred between the CsPbBr₃ and the TPE additives (Figure S9). The average decay time, τ_{avg} , of CsPbBr₃ was 0.85 ns. In the case of PL emission at 535 nm, the CsPbBr₃ films containing TPE at molar ratios of 0.2, 0.4, and 0.6 exhibited τ_{avg} values of 1.78, 1.86, and 2.08 ns, respectively; the CsPbBr₃ films containing BrTPE at molar ratios of 0.2, 0.4, and 0.6 exhibited τ_{avg} values of 4.04, 4.25, and 4.57 ns, respectively; and the CsPbBr₃ films containing TeBrTPE at molar ratios of 0.2, 0.4, and 0.6 exhibited τ_{avg} values of 5.16, 5.29, and 5.55 ns, respectively. Thus, as the TPE derivative content was increased, the decay time increased, indicating that the TPE derivatives interacted with the perovskite material. That is, we inferred that the delay time was longer than the average decay time of the perovskite because of an interaction of the TPE derivatives and the perovskite, where energy is transferred from the large-bandgap TPE derivatives to the perovskite. The third factor is perovskite grain size control and defect passivation. SEM observations revealed that, with decreasing grain size, the number of pinholes decreased. When a perovskite material is used as an efficient light-emitting layer, it is necessary to improve the radiative recombination effect by controlling the crystal grain size of the perovskite. A small crystal grain size enables effective spatial confinement of the excitons, thereby inhibiting the dissociation and diffusion of excitons. Finally, small crystal grains can lead to a PLQY enhancement of the perovskite material [37]. Moreover, when an AIE organic compound is added, PLQY enhancement through defect passivation can be confirmed.

3.4. Implementation of Three-Color White PL Emission in a Double Emitting Layer

Because a perovskite film can be prepared by a solution process and exhibits excellent optical properties, white-light-emitting devices with perovskite and organic light-emitting materials are being actively developed. However, blue-light-emitting perovskite materials exhibit weak luminous efficiency and poor stability compared with red- and green-light-emitting perovskite materials [11,41]. In addition, the emission band of blue-light emitting perovskites has a narrow FWHM, making white-light emission difficult. However, TPE derivatives have stable light emission in the blue region and the FWHM of their emission band is wider than that of perovskite materials; thus, the use of perovskite and TPE materials together should be advantageous in realizing white-light emission.

To achieve ideal white-light emission on the basis of the results of the present study, we prepared a perovskite film with a TeBrTPE/CsPbBr₃ molar ratio of 0.4, which had a high PLQY as well as 1:1 ratio of blue and green PL intensities. We then vacuum-deposited a red phosphorescent material, 4,4'-Bis(N-carbazolyl)-1,1'-biphenyl (CBP): 9 wt% Ir(piq)₃, on top of the perovskite film with TeBrTPE (0.4 molar ratio) to achieve a thickness of 20 nm, resulting in a double emitting layer. This film exhibited three-color white PL emission with a CIE value of (0.25, 0.36) as shown in Figure 6. By applying an organic light-emitting ligand with an AIE moiety to a perovskite material, we improved the luminous efficiency of CsPbBr₃, suggesting that a three-color white LED device was feasible. Further studies on a three-color white LED are underway.

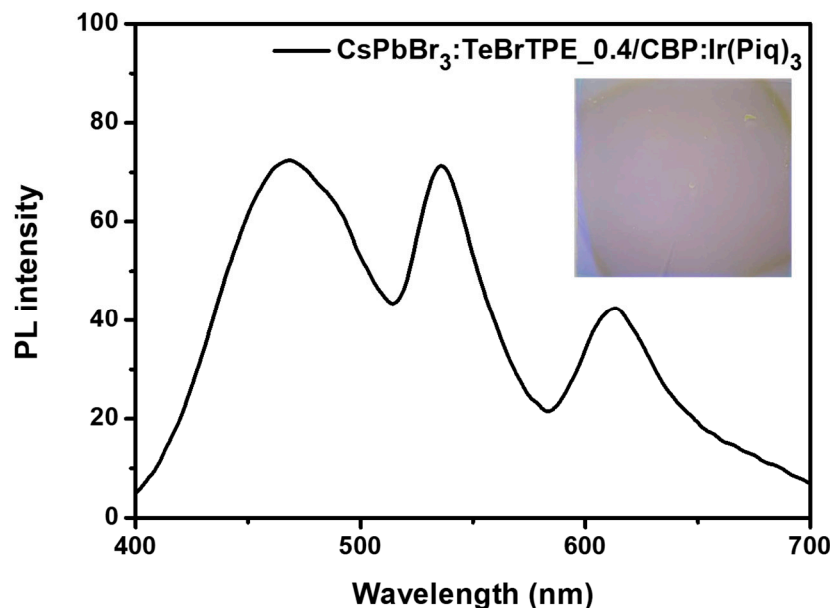


Figure 6. White-light PL spectrum of a vacuum-deposited film of a red emitter on a CsPbBr₃ film with a BrTPE/CsPbBr₃ molar ratio of 0.4 (excitation wavelength: 300 nm), inset: optical photograph under irradiation of 365 nm.

4. Conclusions

By applying an organic light-emitting ligand with AIE characteristics to CsPbBr₃ at various molar ratios, we improved the luminous efficiency of the perovskite light-emitting material and obtained a film that simultaneously emitted green and blue light. The role of the AIE effect and the number of substituted halides in the TPE derivatives was investigated to improve the luminescence efficiency as well as the passivation effect resulting from the small grain size and ligand interaction of the perovskite material. The CsPbBr₃ films were prepared using a nanocrystal-pinning solution mixed with TPE derivatives at different molar ratios of 0.2 to 0.6. When TeBrTPE was added to the CsPbBr₃ film at a molar ratio of 0.6, the PLQY value of CsPbBr₃ was 18.6%, which was approximately 47 times higher than the PLQY value of pure CsPbBr₃ (0.4%). In particular, when TeBrTPE was added, the crystallinity of the CsPbBr₃ was substantially increased. We confirmed that the interaction of the perovskite crystal domain as well as the PL intensity of CsPbBr₃ were increased. As a result, upon deposition of a red phosphorescent material, CBP:Ir(piq)₃, onto a CsPbBr₃ film with a TeBrTPE/CsPbBr₃ molar ratio of 0.4, which exhibited high PL efficiency, three distinct wavelengths of 469, 535, and 613 nm in the double layer were observed. This double-layer film also exhibited three-color white-light PL emission with a CIE value of (0.25, 0.36).

Supplementary Materials: The following supporting information can be downloaded at: <https://www.mdpi.com/article/10.3390/molecules27133982/s1>, Scheme S1: Synthetic route of TPE derivatives. Figure S1: ¹HNMR spectra of BrTPE. Figure S2: ¹³CNMR spectra of BrTPE. Figure S3: ¹HNMR spectra of TeBrTPE. Figure S4: ¹³CNMR spectra of TeBrTPE. Figure S5: Fluorescence spectra of TPE derivatives measured in THF-water of different vol%. (a) TPE, (b) TPEBr, (c) TeBrTPE, and (d) fluorescence intensity changes of TPE, BrTPE, TeBrTPE (excitation: 300 nm). Figure S6: Fluorescence photographs of TPE derivatives measured in different vol% of THF-water (excitation: 365 nm). Figure S7: Fluorescence photographs of CsPbBr₃ films containing TPE derivatives/CsPbBr₃ molar ratios of 0.2, 0.4, and 0.6 (excitation: 365 nm): (a) TPE, (b) BrTPE, and (c) TeBrTPE. Figure S8: PL spectra of CsPbBr₃ films including various molar ratio of 9,10-DBA (Excitation: 365 nm). Figure S9: PL decay profiles of the CsPbBr₃ films including 0.2-0.6 molar ratio of TPE derivatives. (a) TPE, (b) BrTPE, and (c) TeBrTPE (Excitation: 365 nm, emission 535 nm). Equation: The average lifetimes of the emission decay.

Author Contributions: Conceptualization, H.K., S.K. and J.P.; methodology, S.P.; validation, H.K. and S.K.; formal analysis, H.K., H.L. and J.P.; investigation, S.P. and S.K.; resources, J.P.; writing—original draft preparation, H.K. and S.P.; writing—review and editing, H.L. and J.P.; visualization, S.P. and H.L.; supervision, J.P.; project administration, J.P.; funding acquisition, J.P. All authors have read and agreed to the published version of the manuscript.

Funding: This research was supported by National R&D Program through the National Research Foundation of Korea (NRF) funded by the Ministry of Science & ICT (No. 2020M3A7B4002030). This research was supported by the Basic Science Research Program through the National Research Foundation of Korea (NRF) funded by the Ministry of Education (2020R1A6A1A03048004). This work was supported by the Korea Institute for Advancement of Technology (KIAT) and the Ministry of Trade, Industry & Energy (MOTIE) of the Republic of Korea (No. P0017363). This work was supported by the Technology Innovation Program (Material parts equipment innovation Lab technology development project) (20016813, Development of the ALD precursor with high thermal resistance for improving the dielectric thin film characteristics for DRAM capacitor) funded By the Ministry of Trade, Industry & Energy (MOTIE, Korea). This work was supported by the Korea Basic Science Institute (KBSI) National Research Facilities & Equipment Center (NFEC) grant funded by the Korea government (Ministry of Education) (No. 2019R1A6C1010052).

Institutional Review Board Statement: Not applicable.

Informed Consent Statement: Not applicable.

Data Availability Statement: Not applicable.

Conflicts of Interest: The authors declare no conflict of interest.

Sample Availability: Samples of the compounds are available from the authors.

References

1. Tang, C.W.; Vanslyke, S.A. Organic electroluminescent diodes. *Appl. Phys. Lett.* **1987**, *51*, 913–915. [[CrossRef](#)]
2. Kang, S.; Jung, H.; Lee, H.; Park, S.; Kim, J.; Park, J. Highly efficient dual-core derivatives with EQEs as high as 8.38% at high brightness for OLED blue emitters. *J. Mater. Chem.* **2019**, *7*, 14709–14716. [[CrossRef](#)]
3. Jung, H.C.; Shin, H.G.; Kim, S.; Kim, J.; An, B.; Lee, J.; Iheed, H.; Park, J. High electroluminescence efficiency and long device lifetime of a fluorescent green-light emitter using aggregation-induced emission. *J. Ind. Eng. Chem.* **2020**, *87*, 213–221. [[CrossRef](#)]
4. Zhao, Z.; Deng, C.; Chen, S.; Lam, J.M.Y.; Qin, W.; Lu, P.; Wang, Z.; Kwok, H.S.; Ma, Y.; Qiu, H.; et al. Full emission color tuning in luminogens constructed from tetraphenylethene, benzo-2,1,3-thiadiazole and thiophene building blocks. *Chem. Commun.* **2011**, *47*, 8847–8849. [[CrossRef](#)] [[PubMed](#)]
5. Yang, Y.; Zheng, Y.; Cao, W.; Titov, A.; Hyvonen, J.; Manders, J.R.; Xue, J.; Holloway, P.H.; Qian, L. High-efficiency light-emitting devices based on quantum dots with tailored nanostructures. *Nat. Photonics* **2015**, *9*, 259–266. [[CrossRef](#)]
6. Kokima, A.; Teschima, K.; Shirai, Y.; Miyasaka, T. Organometal Halide Perovskites as Visible-Light Sensitizers for Photovoltaic Cells. *J. Am. Chem. Soc.* **2009**, *131*, 6050. [[CrossRef](#)]
7. Akkerman, Q.A.; D’Innocenzo, V.; Accornero, S.; Scarpellini, A.; Petrozzan, A.; Prato, M.; Manna, L. Tuning the Optical Properties of Cesium Lead Halide Perovskite Nanocrystals by Anion Exchange Reactions. *J. Am. Chem. Soc.* **2015**, *137*, 10276–10281. [[CrossRef](#)]
8. Zou, W.; Li, R.; Zhang, S.; Liu, Y.; Wang, N.; Cao, Y.; Miao, Y.; Xu, M.; Guo, Q.; Di, D.; et al. Minimising efficiency roll-off in high-brightness perovskite light-emitting diodes. *Nat. Commun.* **2018**, *9*, 608. [[CrossRef](#)]
9. Zhang, D.; Eaton, S.W.; Yu, Y.; Dou, L.; Yang, P. Solution-Phase Synthesis of Cesium Lead Halide Perovskite Nanowires. *J. Am. Chem. Soc.* **2015**, *137*, 9230–9233. [[CrossRef](#)]
10. Swarnkar, A.; Chulliyil, R.; Ravi, V.K.; Irfanullah, M.; Chowdhury, A.; Nag, A. Colloidal CsPbBr₃ Perovskite Nanocrystals: Luminescence beyond Traditional Quantum Dots. *Angew. Chem.* **2015**, *127*, 15644–15648. [[CrossRef](#)]
11. Kang, S.; Park, S.; Kwon, H.; Lee, J.; Hong, K.-H.; Pu, Y.-J.; Park, J. Achieving green and deep-blue perovskite LEDs by dimensional control using various ammonium bromides with CsPbBr₃. *Mater. Today Energy* **2021**, *21*, 100749. [[CrossRef](#)]
12. Jang, J.; Kim, Y.-H.; Park, S.; Yoo, D.; Cho, H.; Jang, J.; Jeong, H.B.; Lee, H.; Yuk, J.M.; Park, C.B.; et al. Extremely Stable Luminescent Crosslinked Perovskite Nanoparticles under Harsh Environments over 1.5 Years. *Adv. Mater.* **2021**, *33*, 2005255. [[CrossRef](#)]
13. Lee, J.Y.; Kim, S.Y.; Yoon, H.J. Small Molecule Approach to Passivate Undercoordinated Ions in Perovskite Light Emitting Diodes: Progress and Challenges. *Adv. Opt. Mater.* **2022**, *10*, 210361. [[CrossRef](#)]
14. Lee, S.; Park, J.H.; Lee, B.R.; Jung, E.D.; Yu, J.C.; Nuzzo, D.D.; Friend, R.H.; Song, M.H. Amine-Based Passivating Materials for Enhanced Optical Properties and Performance of Organic–Inorganic Perovskites in Light-Emitting Diodes. *J. Phys. Chem. Lett.* **2017**, *8*, 1784–1792. [[CrossRef](#)]

15. Wang, N.; Cheng, L.; Si, J.; Liang, X.; Jin, Y.; Wang, J.; Huang, W. Morphology control of perovskite light-emitting diodes by using amino acid self-assembled monolayers. *Appl. Phys. Lett.* **2016**, *108*, 141102. [[CrossRef](#)]
16. Tang, L.; Qiu, Z.; Wei, Q.; Gu, H.; Du, B.; Du, H.; Hui, W.; Xia, Y.; Chen, Y.; Huang, W. Enhanced Performance of Perovskite Light-Emitting Diodes via Diamine Interface Modification. *ACS Appl. Mater. Interfaces* **2019**, *11*, 29132–29138. [[CrossRef](#)]
17. Yuan, F.; Ran, C.; Zhang, L.; Dong, H.; Jiao, B.; Hou, X.; Li, J.; Wu, Z. A Cocktail of Multiple Cations in Inorganic Halide Perovskite toward Efficient and Highly Stable Blue Light-Emitting Diodes. *ACS Energy Lett.* **2020**, *5*, 1062–1069. [[CrossRef](#)]
18. Friend, R.H.; Gymer, R.W.; Holmes, A.B.; Burroughes, J.H.; Marks, R.N.; Taliani, C.; Bradley, D.D.C.; Dos Santos, D.A.; Brédas, J.L.; Lögdlund, M.; et al. Electroluminescence in conjugated polymers. *Nature* **1999**, *397*, 121–128. [[CrossRef](#)]
19. Jenekhe, S.A.; Osaheni, J.A. Excimers and Exciplexes of Conjugated Polymers. *Science* **1994**, *265*, 765–768. [[CrossRef](#)]
20. Yan, D.; Wu, Q.; Wang, D.; Tang, B.Z. Innovative Synthetic Procedures for Luminogens Showing Aggregation-Induced Emission. *Angew. Chem.* **2020**, *60*, 15724–15742. [[CrossRef](#)]
21. Tong, H.; Hong, Y.; Dong, Y.; Häußler, M.; Lam, J.W.Y.; Li, Z.; Guo, Z.; Guo, Z.; Tang, B.Z. Fluorescent “light-up” bioprobes based on tetraphenylethylene derivatives with aggregation-induced emission characteristics. *Chem. Commun.* **2006**, *35*, 3705–3707. [[CrossRef](#)] [[PubMed](#)]
22. Luo, J.; Xie, Z.; Lam, J.W.Y.; Cheng, L.; Chen, H.; Qui, C.; Kwok, H.S.; Zhan, X.; Liu, Y.; Zhu, D.; et al. Aggregation-induced emission of 1-methyl-1,2,3,4,5-pentaphenylsilole. *Chem. Commun.* **2001**, *18*, 1740–1741. [[CrossRef](#)] [[PubMed](#)]
23. Chen, J.; Xie, Z.; Lam, J.W.Y.; Law, C.C.W.; Tang, B.Z. Silole-Containing Polyacetylenes. Synthesis, Thermal Stability, Light Emission, Nanodimensional Aggregation, and Restricted Intramolecular Rotation. *Macromolecules* **2003**, *36*, 1108–1117. [[CrossRef](#)]
24. Hu, Z.; Zhang, H.; Chen, Y.; Wang, Q.; Elesegood, M.R.J.; Teat, S.J.; Feng, X.; Islam, M.M.; Wu, F.; Tang, B.Z. Tetraphenylethylene-based color-tunable AIE-ESIPT chromophores. *Dyes Pigment.* **2020**, *175*, 108175. [[CrossRef](#)]
25. Yang, Z.; Famg, M.; Li, Z. Organic luminescent materials: The concentration on aggregates from aggregation-induced emission. *Aggregate* **2020**, *1*, 6–18. [[CrossRef](#)]
26. Hwang, J.; Nagaraju, P.; Cho, M.J.; Choi, D.H. Aggregation-induced emission luminogens for organic light-emitting diodes with a single-component emitting layer. *Aggregate* **2022**, e199. [[CrossRef](#)]
27. Yang, Y.; Li, Q.; Zhang, H.; Liu, H.; Ji, X.; Tang, B.Z. Codes in Code: AIE Supramolecular Adhesive Hydrogels Store Huge Amounts of Information. *Adv. Mater.* **2021**, *33*, 2105418. [[CrossRef](#)]
28. Guan, Z.; Li, Y.; Zhu, Z.; Zeng, Z.; Shen, D.; Tan, J.; Tang, S.-W.; Liu, S.; Lee, C.-S. Efficient Perovskite White Light-Emitting Diode Based on an Interfacial Charge-Confinement Structure. *ACS Appl. Mater. Interfaces* **2020**, *30*, 2001732. [[CrossRef](#)]
29. Yao, E.-P.; Yang, Z.; Meng, L.; Sun, P.; Dong, S.; Yang, Y.; Yang, Y. High-Brightness Blue and White LEDs based on Inorganic Perovskite Nanocrystals and their Composites. *Adv. Mater.* **2017**, *29*, 1606859. [[CrossRef](#)]
30. Mao, J.; Lin, H.; Ye, F.; Qin, M.; Burkhartsmeyer, J.M.; Zhang, H.; Lu, X.; Wong, K.S.; Chong, W.C.H. All-Perovskite Emission Architecture for White Light-Emitting Diodes. *ACS Nano* **2018**, *12*, 10486–10492. [[CrossRef](#)]
31. Kwon, H.; Park, S.; Kang, S.; Park, S.; Park, J. Three-color white electroluminescence emission using perovskite quantum dots and organic emitters. *Appl. Surf. Sci.* **2022**, *588*, 152875. [[CrossRef](#)]
32. Chang, C.-Y.; Solodukhin, A.N.; Liao, S.-Y.; Mahesh, K.P.O.; Hsu, C.-L.; Ponomarenko, S.A.; Luponosov, Y.N.; Chao, Y.-C. Perovskite white light-emitting diodes based on a molecular blend perovskite emissive layer. *J. Mater. Chem. C* **2019**, *7*, 8634–8642. [[CrossRef](#)]
33. Wei, Z.; Wei, Z.; Lingyun, L.; Ping, H.; Zhongliang, G.; Ziwei, Z.; Jinyue, S.; Yan, Y.; Xueyuan, C. Dual-Band-Tunable White-Light Emission from Bi³⁺/Te⁴⁺ Emitters in Perovskite-Derivative Cs₂SnCl₆ Microcrystals. *Angew. Chem.* **2022**, *61*, e202116085.
34. Li, Q.; Jin, X.; Song, Y.; Zhang, Q.; Xu, Z.; Chen, Z.; Cheng, Y.; Luo, X. Random Terpolymer Designed with Tunable Fluorescence Lifetime for Efficient Organic/Inorganic Hybrid Solar Cells. *ACS Appl. Mater. Interfaces* **2015**, *7*, 17408–17415. [[CrossRef](#)]
35. Tang, B.Z.; Qin, A. *Aggregation-Induced Emission: Fundamentals*; Wiley: Hoboken, NJ, USA, 2013; pp. 134–150.
36. Li, Z.; Chen, Z.; Yang, Y.; Xue, Q.; Yip, H.L.; Cao, Y. Modulation of recombination zone position for quasi-two-dimensional blue perovskite light-emitting diodes with efficiency exceeding 5. *Nat. Commun.* **2019**, *10*, 1027. [[CrossRef](#)]
37. Chin, S.-H.; Choi, J.W.; Woo, H.C.; Kim, J.H.; Lee, H.S.; Lee, C.-L. Realizing a highly luminescent perovskite thin film by controlling the grain size and crystallinity through solvent vapour annealing. *Nanoscale* **2019**, *11*, 5861–5867. [[CrossRef](#)]
38. Kim, B.W.; Heo, J.H.; Park, J.K.; Lee, D.S.; Park, H.; Kim, S.Y.; Kim, J.H.; Im, S.H. Morphology controlled nanocrystalline CsPbBr₃ thin-film for metal halide perovskite light emitting diodes. *J. Ind. Eng. Chem.* **2021**, *97*, 417–425. [[CrossRef](#)]
39. Song, L.; Guo, X.; Hu, Y.; Lv, Y.; Lin, J.; Liu, Z.; Fan, Y.; Xin, L. Efficient Inorganic Perovskite Light-Emitting Diodes with Polyethylene Glycol Passivated Ultrathin CsPbBr₃ Films. *J. Phys. Chem. Lett.* **2017**, *8*, 4148–4154. [[CrossRef](#)]
40. Lee, G.; Lee, S.Y.; Park, S.; Jang, S.H.; Park, H.-K.; Choi, I.; Park, J.; Choi, J. Highly Effective Surface Defect Passivation of Perovskite Quantum Dots for Excellent Optoelectronic Properties. *J. Mater. Res. Technol.* **2022**, *18*, 4145–4155. [[CrossRef](#)]
41. Baek, S.; Kang, S.; Son, C.; Shin, S.J.; Kim, J.H.; Park, J.; Kim, S.-W. Highly Stable All-Inorganic Perovskite Quantum Dots Using a ZnX₂-Triocetylphosphine-Oxide: Application for High-Performance Full-Color Light-Emitting Diode. *Adv. Opt. Mater.* **2020**, *8*, 1901879. [[CrossRef](#)]
42. Xing, Z.; Zhao, Y.; Askerka, M.; Quan, L.N.; Gong, X.; Zhao, W.; Zhao, J.; Tan, H.; Long, G.; Gao, L.; et al. Color-stable highly luminescent sky-blue perovskite light-emitting diodes. *Nat. Commun.* **2018**, *9*, 3541. [[CrossRef](#)] [[PubMed](#)]
43. Zhang, C.; Wan, Q.; Wang, B.; Zheng, W.; Liu, M.; Zhang, Q.; Kong, L.; Li, L. Surface Ligand Engineering toward Brightly Luminescent and Stable Cesium Lead Halide Perovskite Nanoplatelets for Efficient Blue- Light-Emitting Diodes. *J. Phys. Chem. C* **2019**, *123*, 26161–26169. [[CrossRef](#)]